Advancements in measuring the wall-normal velocity fluctuations in a turbulent boundary layer

Clayton P. Byers

Dept. of Mechanical and Aerospace Engineering
Princeton University
Princeton, NJ 08544, United States
claytonb@princeton.edu

Matthew K. Fu

Dept. of Mechanical and Aerospace Engineering
Princeton University
Princeton, NJ 08544, United States
mkfu@princeton.edu

Yuyang F. Fan

Dept. of Mechanical and Aerospace Engineering
Princeton University
Princeton, NJ 08544, United States
yf@princeton.edu

Katherine A. Kokmanian

Dept. of Mechanical and Aerospace Engineering
Princeton University
Princeton, NJ 08544, United States
kkokmanian@princeton.edu

Marcus N. Hultmark

Dept. of Mechanical and Aerospace Engineering
Princeton University
Princeton, NJ 08544, United States
hultmark@princeton.edu

ABSTRACT

A novel velocity sensor has been developed and characterized for use in turbulent flows. The new strain-based sensor uses a free-standing nano-ribbon exposed to the flow, which results in a geometrically determined sensitivity to a single velocity component. A nano-ribbon deflects under the action of fluid forcing, causing an internal strain which can be calibrated to the fluid velocity. An anisotropic sensitivity to forcing enables measurements of turbulent fluctuations orthogonal to the free-stream flow using only one sensing element. The sensor is deployed in a turbulent boundary layer, with sensitivity to fluctuations in the wall-normal direction. Operation of the sensor is simple and, in contrast to constant temperature hot-wire anemometry, does not require a feedback circuit. The predicted frequency response is $\mathcal{O}(10^5)Hz$, making the sensor an interesting alternative for turbulence measurements.

MOTIVATION

Acquiring unattenuated measurements of the full Reynolds stress tensor continues to be a challenge, especially at high Reynolds numbers. Spatial and temporal resolutions are critical for accurate measurements and conventional instrumentation often lacks both. Measurements of turbulent statistics, such as $\overline{u'^2}$, $\overline{v'^2}$, and $\overline{u'v'}$ are often performed using Particle Image Velocimetry (PIV), Laser Doppler Velocimetry (LDV) or multi-component crossed hot-wires. In addition to lacking sufficient resolution at high Reynolds numbers, these measurement techniques are often expensive and can be complicated to use, prohibiting many researchers from employing them. As noted by De Graaff & Eaton (2000), obtaining the wall-normal fluctuating velocity is a difficult prospect. Here, we present the first measurements in a turbulent boundary layer using Elastic Filament Velocimetry (EFV). The EFV technology was first described by Fu *et al.* (2016) and holds an advantage both in its operational simplicity, only requiring a Wheatstone bridge to obtain measurements, and in its spatial and temporal resolutions.

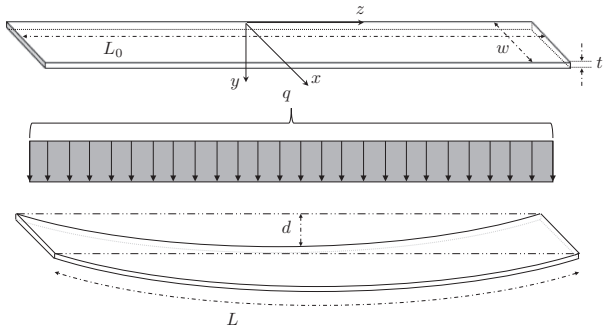

(a) Geometry of the EFV sensing wire with unstretched length L_0, stretched length L, width w, thickness t, centerline deflection d, and fluid force per unit span q. Figure adapted from Fu *et al.* (2016).

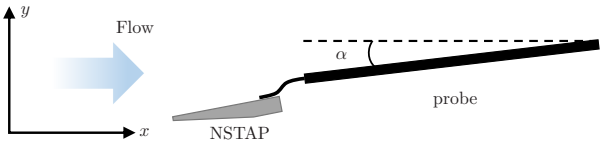

(b) Sensor setup in the flow with angle of attack α relative to the flow direction. A value of $\alpha = 0^\circ$ corresponds to the sensor straight into the flow, solder side up, and $\alpha = 90^\circ$ corresponds to the solder side facing the flow.

Figure 1: Geometry of the sensing element in the experiment.

THEORY OF OPERATION

EFV obtains velocity measurements by correlating the strain in a nano-ribbon to the fluid velocity. By considering the geometry in figure 1a, the centerline deflection in the nano-ribbon, d, is much greater the thickness of the wire, t, leading to a non-linear stretching mode of operation where the classic Euler-Bernoulli beam theory is no longer valid.

Using a design based on previous nanoscale flow sensors developed at Princeton such as the nanoscale thermal anemometry probe, the NSTAP, and its cold-wire equivalent, the T-NSTAP (see Fan *et al.*, 2015), the EFV sensing element will enable centerline deflections on the order of $d = 1$ to $10\mu m$ when exposed to flow.

From these geometric conditions, an order-of-magnitude analysis of the governing beam equation, as shown in Fu *et al.* (2016), then gives the following low order model for the axial strain within the sensing wire, ε, and centerline deflection as:

$$\varepsilon \propto \frac{d^2}{L_0^2} \propto \left(\frac{qL_0}{EA}\right)^{2/3} \tag{1}$$

where q is the force per unit span from the fluid flow, L_0 is the unstrained length of the sensing wire, E is the modulus of elasticity of the wire and A is the cross-sectional area of the wire, given by $A = wt$, where w and t represent the wire width and thickness, respectively. The fluid forcing is due to the drag on the wire, and in the low Reynolds number operation ($Re = \mathcal{O}(1)$), we can express the fluid forcing as:

$$q = C_D \mu U_c \tag{2}$$

where C_D is the Stokes drag coefficient, μ is the dynamic viscosity of the fluid and U_c is the velocity of the fluid acting across the sensor.

By combining equations (1) and (2), the strain is fully predicted by the material properties, the geometry, and the flow around the sensor. Velocity measurements can then be obtained by relating strain to a resistance change with the following relation:

$$\frac{\Delta R}{R_0} = G_F \cdot \varepsilon \tag{3}$$

where ΔR is the change in wire resistance, R_0 is the resistance of the unstrained wire, and G_F is the material dependent gauge factor. The relations in equations (1) to (3) allow a prediction of the wire output as a function of fluid forcing. Based on the results of Fu *et al.* (2016), the change in resistance can be predicted as:

$$\frac{\Delta R}{R_0} = 1.2\left(\frac{C_D \mu U_c L_0}{\sqrt{3}EA}\right)^{2/3} \tag{4}$$

A normalized pre-deflection to the wire, σ_0^+, can be introduced to modify equation (4), as explained in the appendix of Fu *et al.* (2016).

To estimate the dynamic response of the EFV to a turbulent flow, the local deflection of the EFV is modeled using a leading order approximation of the Timoshenko beam equation (Howson & Williams, 1973) with viscous fluid forcing resulting in a modified version of the Morison equation (Morison *et al.*, 1950). An order-of-magnitude analysis gives a damping time scale, T, as:

$$T = \frac{\rho_w A}{C_D \mu} \tag{5}$$

where ρ_w is the density of the wire. Utilizing the geometric and material parameters of the NSTAP, the timescale to fluid forcing is estimated at $5\mu s$, or $200kHz$, which is faster than most available technologies, and is more than sufficient in the turbulent boundary layer to be studied herein.

SENSOR CAPABILITIES

To evaluate the scaling theory, the EFV sensor was subjected to fluid forcing from both water and air under a number of different geometries. The coefficient of drag was determined using 2-D laminar flow simulations over a rectangular cross-section and the gauge factor was determined to be 2.4 by correlating resistance response to the observed deflections measured through confocal microscopy. Initial characterization and testing of the EFV sensor performed by Fu *et al.* (2016) can be seen in figure 2.

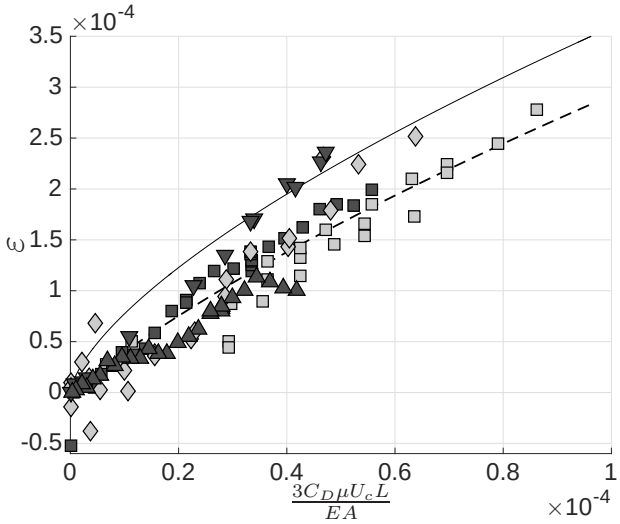

Figure 2: Comparison of the scaling theory for the EFV sensor (solid line) with experimental data of various wire and fluid configurations. Symbols: $\square$ $750 \times 6.5\mu m$, $\diamond$ $750 \times 6.5\mu m$ (from confocal microscopy), $\triangle$ $375 \times 6.5\mu m$, $\triangledown$ $375 \times 2.5\mu m$. Dark gray symbols for measurements in water, light gray symbols for air. Dashed line includes a finite pre-deflection σ_0^+ of the wire in the theoretical calculation. Figure adapted from Fu *et al.* (2016).

The data closely follows the scaling theory which includes a finite pre-deflection in the wire. This initial deflection was observed in the wires after manufacture and is a consequence of the method in which the wires are released from the supporting substrate.

The original design of the EFV sensor utilized platinum as the wire material due to the manufacturing experience gained in the NSTAP development. While the sensor functioned as expected and was able to confirm the theory, platinum has a high sensitivity to temperature, which manifests itself as the spread in the data of figure 2. As shown in Fu *et al.* (2016), a change of the fluid temperature of 0.005 $^\circ C$ can result in a shift in the measured strain by approximately 0.0001, which results in the spread of the initial sensor data. For the current study, the EFV is deployed in a large water channel which reduces these temperature effects, as the larger volume of water substantially reduces the temperature fluctuations compared to the small scale test facility utilized in Fu *et al.* (2016).

For the collection of the data in this study, an NSTAP with a wire geometry of $L_0 = 60\mu m$, $w = 2\mu m$ and $t = 0.1\mu m$ has been utilized. While the NSTAP is traditionally operated as a hot-wire in a constant temperature circuit, this study will utilize the EFV effect by using a Wheatstone bridge, with the sensor as one leg, and passing a small current through the sensor. With proper resistor selection for the top two components of the bridge, the current can be approximated as constant throughout the range of velocities, greatly simplifying the calculations in the analysis.

BOUNDARY LAYER FACILITY

The sensor was deployed in a recirculating water channel which is filled with deionized water. A turbulent boundary layer is allowed to develop on the floor of the test section. The test section is $1m \times 0.2m \times 0.15m$, equipped with a $0.45mm$ triangular grid trip at the leading edge to facilitate the development of a fully turbulent boundary layer. At the measurement location, the boundary layer thickness, δ_{99}, varies from $20mm$ to $14mm$, with an inner length scale, $\eta \equiv \nu u_\tau^{-1}$, on the order of $40\mu m$ down to $5\mu m$, for the cases tested here. The friction velocity, u_τ, is defined in the classical manner with respect to the wall shear stress, τ_w, and fluid density, ρ, as $u_\tau \equiv \sqrt{\tau_w \rho^{-1}}$. This also implies a friction Reynolds number range of $500 < Re_\tau \equiv \delta_{99} u_\tau \nu^{-1} < 2800$. This yields $\ell^+ \equiv L_0 \eta^{-1} = 12$ at the highest Reynolds number.

A linear traverse was installed on the centerline of the test section at a location $0.75m$ downstream from the trip, equipped with a pitot tube and the EFV sensor. The traverse has a displacement resolution of $0.5\mu m$, allowing for accurate measurements of the near-wall region.

The EFV sensor is aligned with the nanoscale dimension in the wall-normal direction, causing the wire to be susceptible to forcing in that direction. By aligning the EFV sensor with an angle of 10° to the wall, the mean streamwise velocity applies a small amount of forcing on the wire that manifests itself as the mean of the signal, while the streamwise fluctuations about that mean will result in changes in the wire resistance an order of magnitude smaller compared to the wall-normal velocity fluctuations. This results in a sensor capable of measuring near-wall measurements of $\overline{v'^2}$ with unprecedented resolution both temporally and spatially.

Concerns about the exact location of the sensing wire due to the flexing of the member are mitigated through the use of a $60\mu m$ long wire. The centerline deflection of the wire is estimated using equation 1, resulting in $d \approx 1\mu m$, well under the viscous length scale of the flow facility to be utilized.

SENSOR CALIBRATION

To calibrate the sensor such that the fluctuations in the strain can be related to the fluctuations in the wall-normal component of velocity, its sensitivity to angle and velocity has to be understood. Here, we present a preliminary methodology, which will allow us to qualitatively judge the sensor's capabilities.

The sensor's angle sensitivity was evaluated by operating at various angles of attack relative to the incoming flow at a constant velocity. Comparisons between angles and velocities are made by examining the normalized change in wire resistance. The resistance of the wire is calculated from the parameters in the Wheatstone bridge and the amplification factors, and corrected for the small thermal drift of the water channel over time, which was measured using a thermocouple in the free-stream.

The results of the angle test, as seen in figure 3, show that the sensor has a linear response to angles near $\alpha = 0^\circ$, which is anticipated for small angles from geometric reasoning. However, it was noted that the sensor must be deployed at a moderately positive α to ensure that the wire does not encounter a negative angle of attack relative to the instantaneous flow, which could lead to buckling of any pre-deformation of the wire. Data for $\alpha < -15^\circ$ was not obtained, as the wire experienced such non-linear behavior which can result in electrical drift over time. By deploying the NSTAP in the flow at a small α, the mean flow exerts a nominal strain on the wire that is small enough to avoid plastic deformation, while the wall-normal fluctuations will result in significant fluctuations in the strain. So long as the instantaneous angle of attack does not become significantly negative, there is a linear relation to find the vertical component of velocity.

As hypothesized, the sensor demonstrated significantly higher sensitivity to forcing at 90° compared to the 0° orientation, which can be seen in figure 4. However, it was found that the NSTAP geometry resulted in a bias to the signal at very high angles of attack

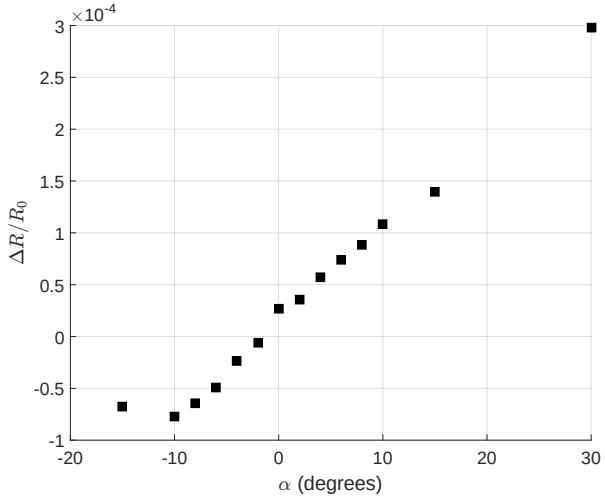

Figure 3: Normalized resistance change in the NSTAP for changing angle at a set speed $U_\infty = 0.39m/s$, with angle α defined from figure 1b.

(greater than 60°) resulting in a smaller strain than predicted geometrically. Since the wall-normal component is applying a force at $\alpha \approx 90^\circ$, yet with a relatively small total angle of attack, this effect is accounted for by using the shape of the calibration curve acquired at 90° and scaling it using the geometrical relationship.

Previous studies of turbulent boundary layers (Fernholz & Finley (1996); De Graaff & Eaton (2000); Jiménez *et al.* (2010); Sillero *et al.* (2013)) have found that the intensity of the wall-normal fluctuations is less than that of the streamwise fluctuations, but within the same order of magnitude. This indicates that the preferential sensing direction will allow the strain to be dominated by the wall-normal component, not the streamwise component. Additionally, there is no characteristic inner or outer peak in the $\overline{v'^2}$ profile and the intensity is suppressed further from the wall compared to streamwise and span-wise fluctuations. These characteristics of the flow field, coupled with the sensitivity indicated in figures 3 and 4, should immediately indicate if the variance is contaminated by streamwise fluctuations.

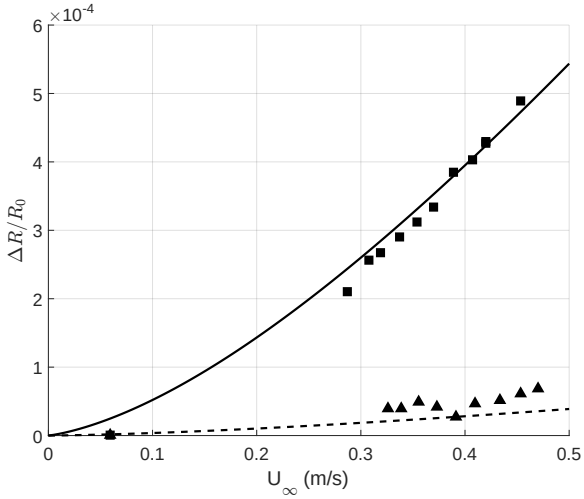

Figure 4: Calibration curve for the NSTAP operating as an EFV. Square symbols (■) taken at $\alpha = 90^\circ$, triangles (▲) at $\alpha = 0^\circ$, as defined in figure 1b. The solid line indicates a curve fit based on equation 6 and the dashed line indicates a correction to the solid line by a factor of 1/14, found experimentally.

Utilizing equation 4, a curve fit for the expected resistance change in the NSTAP can be predicted. Incorporating the pre-deflection factor and the results of Fu *et al.* (2016), this gives a power law behavior:

$$\frac{\Delta R}{R_0} = A \cdot U^{4/3} + B \tag{6}$$

where A and B are constants, and the power of $4/3$ is simply the closest rational expression. The solid line in figure 4 represents this $4/3$ power law fit and shows good agreement with the experimental results of the sensor deployed at 90°, indicated by the (■) symbols. The dashed line in figure 4 takes the ratio of the 90° data with the 0° data, indicated by the (▲) symbols, and applies that factor to the theoretical curve. The results show a good fit, but more importantly demonstrate that there is little sensitivity to the streamwise flow velocity when deployed at low angles of attack.

For the calculation of the wall-normal velocity components, the measured signal is calibrated using the $4/3$ power law. The sensor is deployed in the flow at an angle of attack of $\alpha = 10°$, following the schematic of figure 1b. The scaling factor applied to the $\alpha = 90°$ calibration was determined by the geometrical scaling factor between 100° and 10° which is 5.67, divided by the empirical correction observed in the angle test between 90° and 10°, which was found to be 3.114. This method of calibrating assumes that any forcing from the streamwise velocity fluctuations can be neglected. However, due to the sensor being oriented at 10° there will be a non-zero contribution from these fluctuations.

The effect of the wall-normal measurements being conflated with the streamwise fluctuations are similar to the effect with hot-wire anemometry, which has a signal dominated by the streamwise component of velocity with a small influence in the measurement due to the wall-normal velocity fluctuations.

PRELIMINARY RESULTS

The wall-normal fluctuations as measured by the EFV sensor are shown in figure 5. The data is normalized by the friction velocity u_τ, which is calculated through the use of a Preston tube and the curve fits of Patel (1965) and agrees well with the data of Fernholz & Finley (1996). The wall-normal coordinate is normalized by the boundary layer thickness, determined from a simultaneous measurement from a Pitot tube. Figure 5 also includes the DNS data of Sillero *et al.* (2013) at $Re_\tau = 1307$ for comparison. Qualitatively, the EFV data shares many attributes of the DNS data with similar locations and magnitudes of the maximum fluctuations. However, it is apparent that the EFV is over-predicting the wall-normal fluctuations, compared to the DNS, in the near-wall region. The increased fluctuations measured close to the wall is most likely due to strong streamwise fluctuations in that region, which can introduce artificially high fluctuations, as discussed above.

It should also be pointed out that the current form of the EFV sensor is highly sensitive to temperature. The wire material is platinum, which is highly sensitive to temperature, which means small temperature fluctuations will end up registering as large changes in the signal. The straining of the wire results in a resistance change of 0.1 Ohm over the entire range of velocities in this experiment. Utilizing the measured temperature coefficient of resistance of the wire at $0.002\Delta R(R_0\,^\circ C)^{-1}$, a fluctuation of $0.5^\circ C$ would also register as a 0.1 Ohm change in resistance of the wire. The large volume of water, long warm-up period and long averages help mitigate this potential source of error, but still pose a risk of contaminating the signal.

CONCLUSIONS AND FUTURE WORK

A novel sensor is presented and the preliminary data confirms that the sensor has an anisotropic sensitivity to velocity. By deploying the EFV sensor in a zero pressure gradient turbulent boundary layer, well-resolved measurements of the wall-normal fluctuations, $\overline{v'^2}$, were acquired. However, it was shown that due to the need to operate at a non-zero angle, to avoid buckling of the sensing element, the signal is contaminated by the streamwise velocity component and additional information is needed to truly distinguish the instantaneous magnitude of the velocity from its instantaneous angle. Nonetheless, the results show a promising direction towards obtaining accurate wall-normal velocity fluctuation measurements at an enhanced spatial resolution.

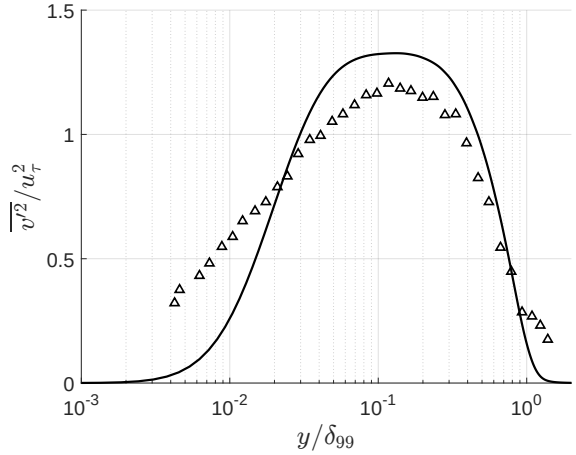

Figure 5: Plot of the data extracted from the EFV sensor at $Re_\tau = 906$ utilizing the theoretical 90° curve of equation 6 and an empirical correction factor. Solid line from Sillero *et al.* (2013) at $Re_\tau = 1307$.

The sensor employed in this study was an NSTAP operated in a cold-wire fashion. By coupling this mode of operation with a high current hot-wire mode, an accurate measurement of the instantaneous velocity could be obtained. This would enable more accurate extraction of the instantaneous angle of the flow, and thus a better calculation of the wall-normal velocity without contamination from the streamwise component. Additionally, coupling the hot- and cold-wire modes would allow a single sensing element to extract multiple Reynolds stresses, including covariance measurements.

REFERENCES

De Graaff, David B & Eaton, John K 2000 Reynolds-number scaling of the flat-plate turbulent boundary layer. *Journal of Fluid Mechanics* **422**, 319–346.

Fan, Y, Arwatz, G, Van Buren, TW, Hoffman, DE & Hultmark, M 2015 Nanoscale sensing devices for turbulence measurements. *Experiments in Fluids* **56** (7), 1–13.

Fernholz, HH & Finley, PJ 1996 The incompressible zero-pressure-gradient turbulent boundary layer: an assessment of the data. *Progress in Aerospace Sciences* **32** (4), 245–311.

Fu, MK, Fan, Y, Byers, CP, Chen, TH, Arnold, CB & Hultmark, M 2016 Elastic filament velocimetry (efv). *Measurement Science and Technology* **28** (2), 025301.

Howson, W. P. & Williams, F. W. 1973 Natural frequencies of frames with axially loaded timoshenko members. *Journal of Sound and Vibration* **26** (4), 503–515.

Jiménez, Javier, Hoyas, Sergio, Simens, Mark P & Mizuno, Yoshinori 2010 Turbulent boundary layers and channels at moderate reynolds numbers. *Journal of Fluid Mechanics* **657**, 335–360.

Morison, J.R., Johnson, J.W. & Schaaf, S.A. 1950 The Force Exerted by Surface Waves on Piles. *Journal of Petroleum Technology* **2** (5), 149–154.

Patel, VC 1965 Calibration of the preston tube and limitations on

its use in pressure gradients. *Journal of Fluid Mechanics* **23** (01), 185–208.

Sillero, Juan A, Jiménez, Javier & Moser, Robert D 2013 One-point statistics for turbulent wall-bounded flows at reynolds numbers up to $\delta+$ 2000. *Physics of Fluids* **25** (10), 105102.